The magnetic field, temperature, strain and angular dependence of the critical current density for Nb-Ti

S B L Chislett-McDonald[1], Y Tsui[1], E Surrey[2], M Kovari[2] and D P Hampshire[1]

[1]Superconductivity Group, Centre for Materials Physics, Department of Physics, Durham University, UK

[2]Culham Centre for Fusion Energy, Culham Science Centre, Abingdon, UK

E-mail: simon.chislett-mcdonald@durham.ac.uk

Abstract. A scaling law for J_c in commercial Nb-Ti wire is proposed that describes its magnetic field, temperature and strain dependence. The scaling law is used to fit extensive measurements of the total strand critical current density, $J_{c,TS}(B, T, \varepsilon)$, with the applied field orthogonal to the axis of the wire. We present critical current density, heat capacity and resistivity measurements to obtain $B^*_{c2}(\theta)$, which shows clear angular anisotropy. At 4.2 K, the resistivity data show $B^*_{c2}(B \parallel J) - B^*_{c2}(B \perp J) \approx 1$ T. We also discuss whether the fusion community should consider re-optimising standard commercial Nb-Ti wires that were developed for MRI applications at ~ 5 T, to produce higher J_c at say 10 T, and higher upper critical fields, perhaps using quaternary Nb-Ti alloys with artificial pinning centres.

1. Introduction

Nb-Ti is the current 'workhorse' of the superconductivity industry. Its ductility, relative ease of manufacture, and low cost make it the natural choice for MRI applications operating up to about 5 T. However, it has been broadly ignored for the highest field parts of any commercial fusion tokamak because it has been seen as unable to produce sufficiently high magnetic field for high fusion gain, Q_{fus}. At 13.5 T, the current designs for EU DEMO [1] demand some toroidal field coils operating at fields greater than the upper critical field, B^*_{c2}, of Nb-Ti (though of course Nb-Ti is incorporated in the low field regions) [2]. However, the recent developments in fusion plasma reactor designs open the possibility of significantly longer plasma energy confinement times, τ_E, [3, 4, 5] than EU DEMO assumes (alternatively described as having large H_{98}-factors). These longer τ_Es reduce the field requirements for a given fusion power output. Primarily this has been viewed as opening an avenue to compact reactors with very high toroidal fields. However it may also open the exciting possibility of commercial fusion reactors that avoid the widespread use of brittle superconductors such as Nb_3Sn and REBCO and predominantly or even exclusively use ductile superconductors such as Nb-Ti alloys [6]. Indeed, as we approach the middle of the 21st century, many large consortia will start to operate large tokamak systems. During this early development, learning and optimisation phase for tokamaks, one can expect to encounter plasma instabilities which produce large intermittent, uncontrolled and unexpected forces on the magnets. Given that demountable coils (and joints), graded conductors and modular magnets (that may need to be replaced every few years) may all be required in any high-availability commercial system, improved Nb-Ti may provide pragmatic ~ 10 T near-term

stepping stone components. After the reliable operation modes/procedures/facilities for the tokamak have been developed, some of these ductile superconducting components can then be replaced by similar-sized higher-field brittle superconductors if necessary. Hence as part of the early developmental phase for large tokamaks, the community will very probably reconsider whether today's commercial (MRI) Nb-Ti wires can be re-optimised for higher field operation in fusion applications. Given that the cost of any Nb-Ti alloy superconductors will probably be a relatively small fraction of the total cost of the tokamak, the total strand critical current density in high magnetic fields will probably be the most important figure of merit.

This paper provides a wide range of measurements made on a commercial single filament wire of Nb-Ti and a commercial multifilamentary Nb-Ti wire. Critical current density, J_c, resistivity, ρ, and heat capacity, C_p, measurements are provided. The data demonstrate that neither the effective upper critical field, B^*_{c2}, for Nb-Ti alloys, nor the critical current density, J_c, are yet fully optimised for operation at the very highest fields, say above $\sim 10\,\mathrm{T}$. We characterise the J_c data using a simple scaling law that includes Bordini et al.'s recent work [7] on the strain dependence of B^*_{c2}. Although the strain dependence of J_c in Nb-Ti wires is sufficiently small that at 5 T it can usually be ignored, in magnetic fields that are close to the upper critical field (i.e. above 10 T), this strain independent approximation breaks down. The scaling law can be used to describe $J_{c,TS}(B, T, \varepsilon)$ at the very highest fields and is particularly useful for computational fusion systems analysis [8] [9]. Finally, we distinguish those measurements of B^*_{c2} that give the properties of the superconductor at its surface from those that give bulk properties and discuss approaches that might improve Nb-Ti alloys for use at the highest fields close to its upper critical field B_{c2}.

2. Terminology

Critical current density is not a thermodynamic variable. It is characterised at an arbitrary electric field criterion, E_c where a typical electric field–current density (E–J) transport measurement is characterised using

$$E = E_c \left(\frac{J}{J_c} \right)^N \tag{1}$$

and N is the index of transition. The architecture of conductors used in superconducting magnets is complex. Figure 2 helps outline the different terminology used for the critical current density. In optimising the current density carrying capacity of the superconducting material itself, $J_{c,\mathrm{Superconductor}}$ is a useful parameter. For REBCO HTS material, it is straightforward to find the cross-sectional area of the superconducting material alone, $\mathrm{Area}_{\mathrm{Superconductor}}$, that is used to calculate $J_{c,\mathrm{Superconductor}} = I_{c,\mathrm{Superconductor}}/\mathrm{Area}_{\mathrm{Superconductor}}$. However for the intermetallic superconductors such as Nb_3Sn, where there can, for example, be the diffusion of tin from bronze into Nb, measuring the thickness of the Nb_3Sn layer can require expensive and time-consuming TEM measurements. The stability of superconducting conductors to electromagnetic and thermal perturbations is broadly determined by the amount of copper in the conductor. Choosing the amount of copper depends on the application. Hence the non-copper J_c, $J_{c,\text{Non-Cu}}$, is a useful characterisation of J_c that is application independent; magnet engineers need to know the critical current density of the whole wire (also known as strand) or tape conductor. They are not usually concerned about the distribution of the current within the conductor itself. This has led to the so-called total strand critical current density $J_{c,TS}$. Equally, fusion magnet designers are concerned about the current density of the entire cable $J_{c,\text{Total Cable}}$. In this paper we quote the total strand critical current density, $J_{c,TS}$, for the Nb-Ti conductors measured.

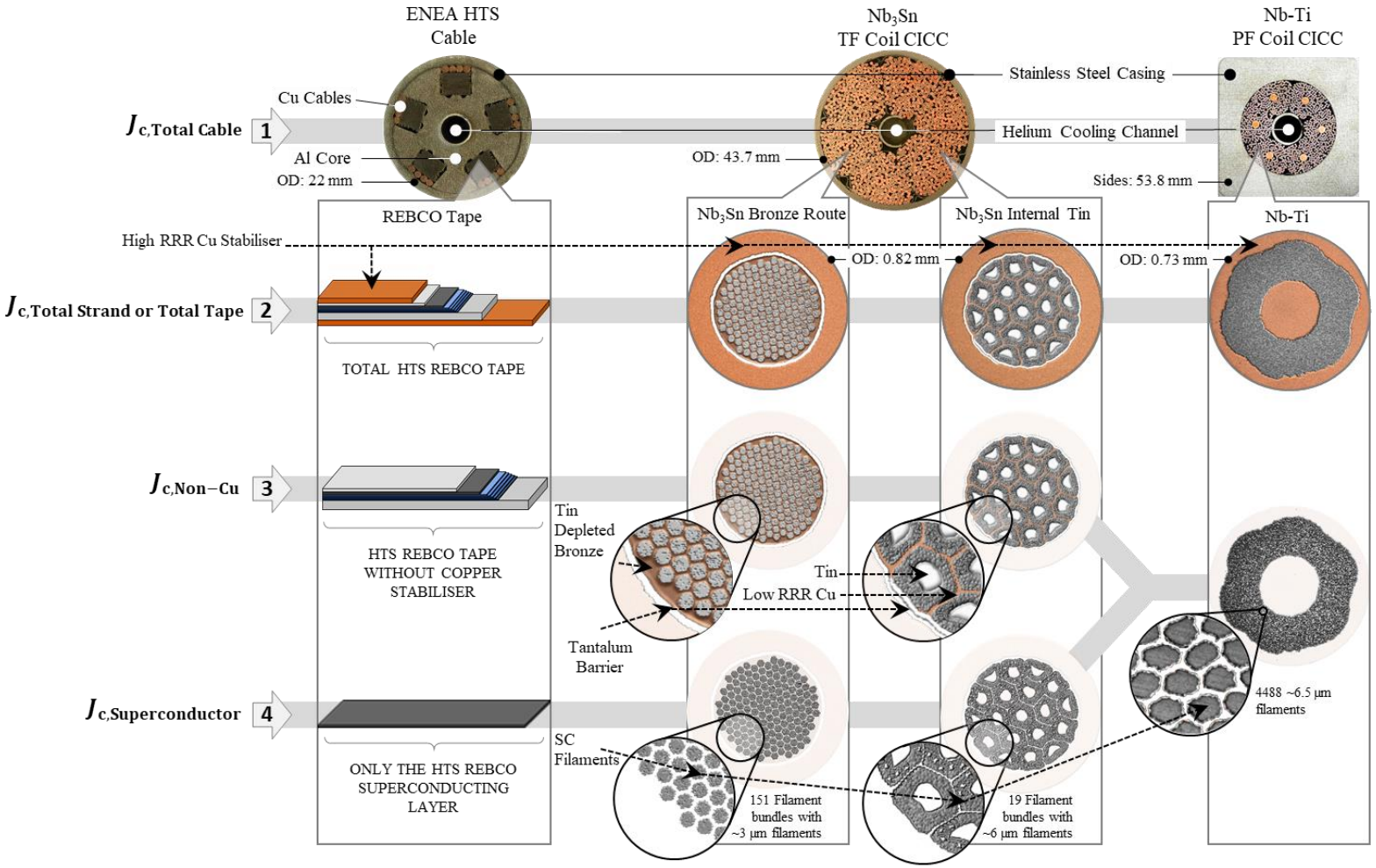

Figure 1. Definitions of the critical current density (the ratio between the critical current, I_c, and the relevant cross-sectional area (CSA)). Row (1): The total CSA of a cable is used i.e. $J_{c,\text{Total Cable}} = I_c/\text{CSA}_{\text{Total Cable}}$. Row (2): The total CSA of a *strand* or *tape* is used i.e. $J_{c,\text{Total Strand or Total Tape}} = I_c/\text{CSA}_{\text{Total strand or Total Tape}}$. Row (3): Only the CSA of the non-copper region is used i.e. $J_{c,\text{Non-Cu}} = I_c/\text{CSA}_{\text{Non-Cu}}$. The CSA of the high RRR (room-temperature resistivity ratio), high purity copper is not included. Row (4): Only the CSA of the superconductor (either total *filament* CSA or the CSA of the *superconducting layer* in a tape) is used i.e. $J_{c,\text{Superconductor}} = I_c/\text{CSA}_{\text{Superconductor}}$. Micrographs for Nb-Ti, Nb_3Sn and images of CICC (Cable-In-Conduit Conductor) cables for these materials [10] [11] and for REBCO [12] are given as examples.

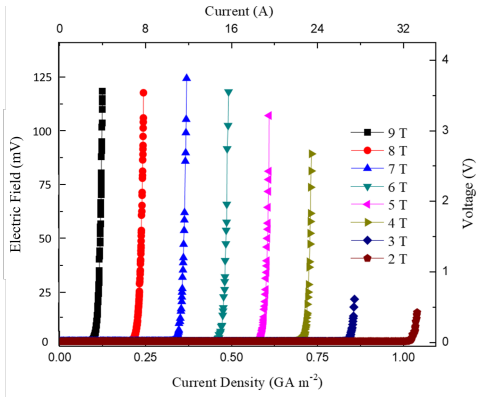

Figure 2. Electric field versus current density (E-J) traces for a single filament Nb-Ti wire at 4.2 K under different fields for $B \perp J$.

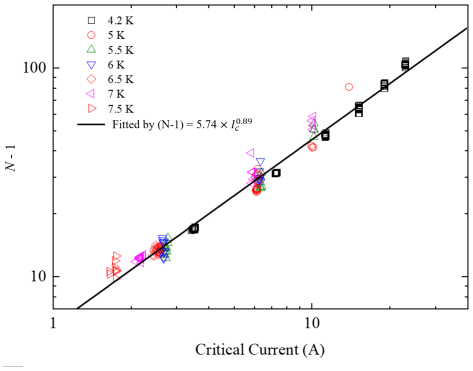

Figure 3. The index of transition or N-value as a function of critical current for a single filament Nb-Ti wire at various fields and temperatures. The N-value is defined in equation 1.

3. Field, temperature and strain dependence of the critical current density

Figures 2 to 6 provide comprehensive $J_{c,TS}$ measurements as a function of field, temperature and strain for a single-filament Nb-Ti conductor. Figure 2 shows some of the typical E - J data that were fitted with equation 1 to find the N-values shown in figure 3 and $J_{c,TS}$ shown in figure 4. Figure 5 shows $J_{c,TS}$ measured with the field either orthogonal or parallel to the axis of the wire. These $J_{c,TS}$ data show that the bulk properties of the wire are anisotropic and in particular the upper critical field changes by about 1 T between the two orientations at 4.2 K. The wire was originally a 0.4 mm diameter wire that was cold-drawn down for us to 0.2 mm diameter and is denoted in this paper hereafter using 'as-supplied'. The manufacturers original critical current and N-value specifications at 4.2 K and 5 T were 81 A and $N = 85$ respectively. After cold-drawing the wire, the values were measured to be 19.2 A and $N = 85$, consistent with a simple reduction in the diameter of the superconducting wire by a factor of two. Variable

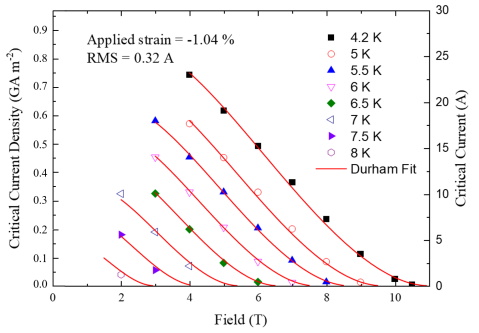

Figure 4. Total strand critical current density for a single filament Nb-Ti wire as a function of field at various temperatures. The two (indistinguishable) solid lines are a standard scaling law with either the global polynomial or exponential fit.

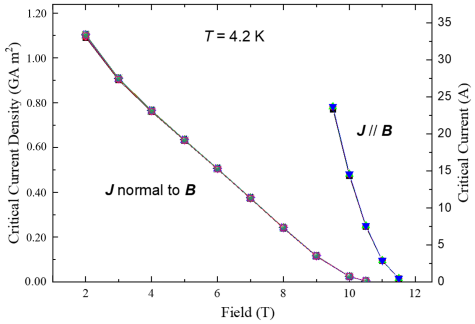

Figure 5. Total strand critical current at 4.2 K of a single filament Nb-Ti wire as a function of applied magnetic field.

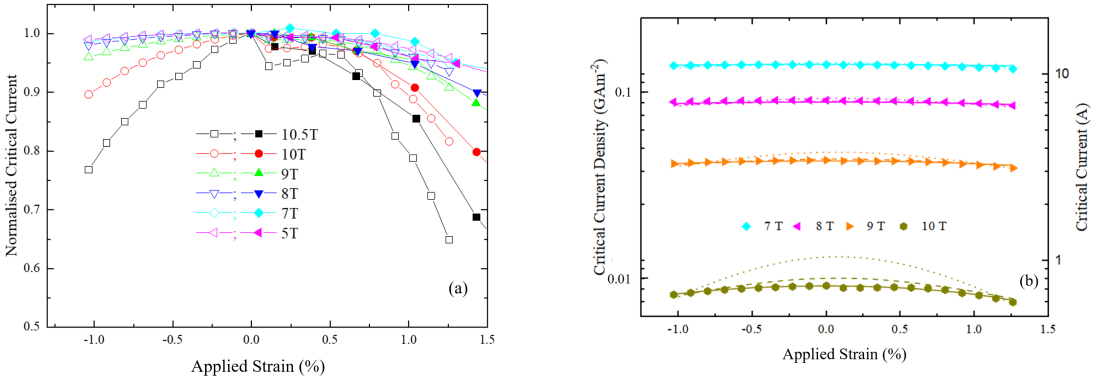

Figure 6. (a) Normalised critical current of a single filament Nb-Ti wire as a function of intrinsic strain at different fields. Closed symbols data are taken from reference [13] (b) Total strand critical current density as a function of applied strain at 4.2 K for different applied fields perpendicular to the direction of current flow. The solid lines are fit using the polynomial dependence for B^*_{c2} (the global and technological fits are indistinguishable). The dotted lines are a global fit using the exponential model of Bordini, the dashed lines are the so-called technological fit using Bordini's model when the fit is weighted preferentially for the low temperature, high field, high strain data.

strain measurements of $J_{c,TS}$ at 4.2 K in high fields for the single filament Nb-Ti are shown in figure 6 made using a Walters spring [14]. For measurements on Nb_3Sn [15], the Nb_3Sn is wound on a mandrel that is shaped like the spring in its unreacted state and then reacted. It therefore fits onto the spring without applying any strain to it. In a multifilamentary Nb-Ti wire considerable strain would be applied when winding and mounting it to a Walters spring. In such a sample, the filaments would be significantly compressed on the inboard side of the wire and significantly tensioned on the outboard side while soldering the wire to the spring. Such an effect is minimised by our choice to measure a small single filament wire because the filament lies on the neutral axis. Figure 7 shows resistivity measurements taken at 4.2 K at different strains under swept field conditions. The changes in B^*_{c2} are small but well above the uncertainties in these measurements.

4. Fit to the critical current of Nb-Ti

The critical current data for the single filament wire were fit to a standard scaling law [16, 17, 18] which is derived from the well-known equation for flux pinning

$$F_p = J_c B = A \frac{[B^*_{c2}(T,\varepsilon)]^n}{(2\pi\Phi_0)^{1/2}\,\mu_0\,[\kappa^*_1(T,\varepsilon)]^2} b^p (1-b)^q \ , \tag{2}$$

where n is a constant, Φ_0 is the flux quantum, ε is the strain, T is the system temperature and κ^*_1 is the effective Ginzburg-Landau parameter [19]. B^*_{c2} can be written as [20]

$$B_{c2}(T,\varepsilon) = \sqrt{2}\kappa^*_1(T,\varepsilon) B_c(T,\varepsilon) \ . \tag{3}$$

From the two fluid model [21] it is known

$$B_c(T) = B_c(0)(1-t^2) \ . \tag{4}$$

From the BCS equation [20] $B_c(0,\varepsilon) \propto T_c$, and extensive measurements have yielded

$$B_{c2}(T,\varepsilon) = B_{c2}(0,\varepsilon)(1-t^\nu) \ . \tag{5}$$

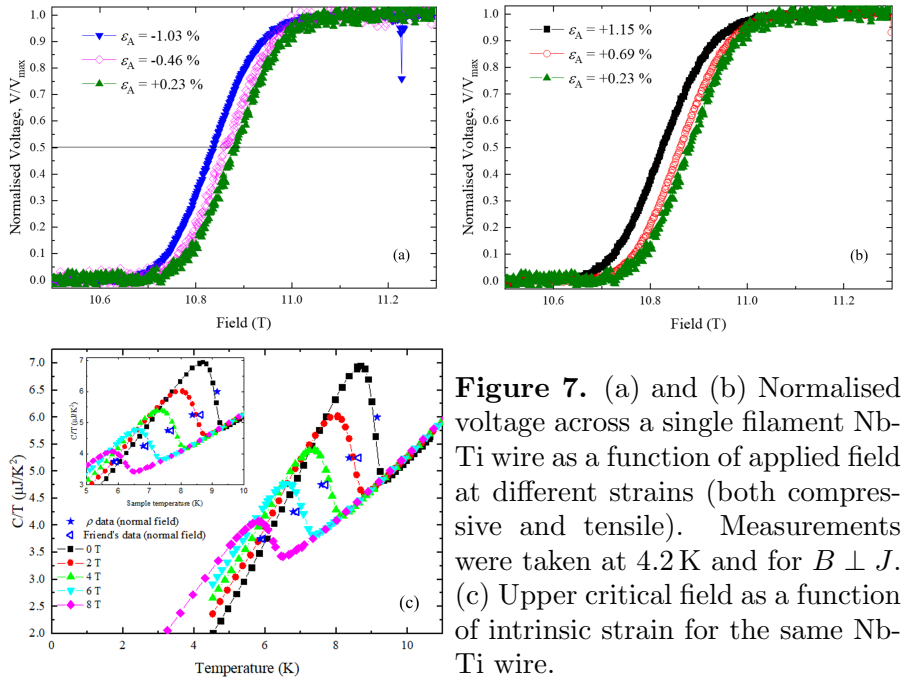

Figure 7. (a) and (b) Normalised voltage across a single filament Nb-Ti wire as a function of applied field at different strains (both compressive and tensile). Measurements were taken at 4.2 K and for $B \perp J$. (c) Upper critical field as a function of intrinsic strain for the same Nb-Ti wire.

Substituting these equations into equation 2, we can write $J_{\mathrm{c,TS}}$ as

$$J_{\mathrm{c,TS}}(B,T,\varepsilon_{\mathrm{I}}) = A^*(\varepsilon)\left[T_{\mathrm{c}}^*(\varepsilon_{\mathrm{I}})(1-t^2)\right]^2\left[B_{\mathrm{c2}}^*(1-t^{\nu})\right]^{n-3}b^{p-1}(1-b)^q\ . \tag{6}$$

The strain dependencies are related through [18]

$$\frac{B_{\mathrm{c2}}^*(0,\varepsilon_{\mathrm{I}})}{B_{\mathrm{c2}}^*(0,0)} = \left(\frac{T_{\mathrm{c}}^*(\varepsilon_{\mathrm{I}})}{T_{\mathrm{c}}^*(0)}\right)^w = \left(\frac{A^*(\varepsilon)}{A^*(0)}\right)^{w/u}\ , \tag{7}$$

and the (applied) strain, ε_{a}, can be written in terms of an intrinsic strain, ε_{I} where

$$\varepsilon_{\mathrm{I}} = \varepsilon_{\mathrm{a}} - \varepsilon_{\mathrm{m}}\ , \tag{8}$$

and ε_{m} is the strain at which the peak in $J_{\mathrm{c,TS}}$ occurs. It has been comprehensively established that these strain scaling laws describe the current density of many different architectures of Nb_3Sn wires. One can relate the strain dependence of T_{c} to the strain dependence B_{c2} through a polynomial [18] given by

$$\frac{B_{\mathrm{c2}}^*(0,\varepsilon_{\mathrm{I}})}{B_{\mathrm{c2}}^*(0,0)} = s(\varepsilon_{\mathrm{I}}) = 1 + c_2\varepsilon_{\mathrm{I}}^2 + c_3\varepsilon_{\mathrm{I}}^3 + c_4\varepsilon_{\mathrm{I}}^4\ . \tag{9}$$

More recently Bordini et al. have proposed an exponential strain model [7]:

$$\frac{B_{\mathrm{c2}}^*(0,\varepsilon_{\mathrm{a}})}{B_{\mathrm{c2}}^*(0,0)} = s(\varepsilon_{\mathrm{a}}) = \frac{\exp\left(-C_{\mathrm{a1}}\frac{J_2+3}{J_2+1}J_2\right) + \exp\left(-C_{\mathrm{a1}}\frac{I_1^2+3}{I_1^2+1}I_1^2\right)}{2}\ , \tag{10}$$

where $I_1 = (1-2\nu_{\text{Nb-Ti}})\varepsilon_{\mathrm{a}} + \varepsilon_{\mathrm{l0}} + 2\varepsilon_{\mathrm{t0}}$ and $J_2 = (\varepsilon_{\mathrm{l0}} - \varepsilon_{\mathrm{t0}} + (1+\nu_{\text{Nb-Ti}})\varepsilon_{\mathrm{a}})^2/3$ and relates the longitudinal residual strain, $\varepsilon_{\mathrm{l0}}$, and the transverse residual strain, $\varepsilon_{\mathrm{t0}}$, through an 'effective'

Table 1. Comparison of the parameters found when fitting a standard scaling law for $J_{c,TS}$ (equation 6) using the polynomial (equation 9) and exponential strain models (equation 10) for $B^*_{c2}(\varepsilon)$ for the data presented in figure 4 and figure 6 for Nb-Ti. A global fit was performed using each scaling law, as well as a high field exponential fit to high field, low temperature data. We compare these data with fits for an bronze-route Nb_3Sn wire [18]. Standard values of $w = 2.2$ and $u = 0$ (equation 7) were fixed for all fits to the Nb-Ti data. The values of p, q, n and ν were fixed for all the Nb-Ti fits to be 1.341, 1.555, 2.274 and 1.758 respectively.

Material (Type of fit)	$A(0)$ ($MAm^{-2}T^{3-n}K^{-2}$)	$T^*_{c,0}$ (K)	$B^*_{c2,0}$ (T)
Nb-Ti (High field exp.)	360.6	7.80	16.00
Nb-Ti (Global exp.)	255.3	8.89	14.67
Nb-Ti (High field poly.)	240.0	8.81	14.50
Nb-Ti (Global poly.)	240.6	8.74	14.61
Nb_3Sn (Global poly.)	213.8	17.10	22.84
Nb_3Sn (Global exp.)	189.1	17.18	24.09

Material (Type of fit)	c_2	c_3	c_4	ε_m (%)	ε_{l0} (%)	C_{a1}
Nb-Ti (High field exp.)	—	—	—	—	0.000	0.007
Nb-Ti (Global exp.)	—	—	—	—	−0.003	0.021
Nb-Ti (High field poly.)	−0.0025	−0.0003	−0.0001	−0.002	—	—
Nb-Ti (Global poly.)	−0.0025	−0.0003	−0.0001	−0.002	—	—
Nb_3Sn (Global poly.)	−0.6602	−0.4656	−0.1075	−0.340	—	—
Nb_3Sn (Global exp.)	—	—	—	—	−0.385	0.356

Poisson's ratio for the Nb-Ti strand $\nu_{\text{Nb-Ti}}$ where $\varepsilon_{t0} = -\nu_{\text{Nb-Ti}}\varepsilon_{l0} + 0.1$ and $\nu_{\text{Nb-Ti}} = 0.33$ [22]. In table 1 the fitting parameters obtained using equation 9 and equation 10 (denoted poly. and exp. in table 1) are provided. The fitting procedure sequence in both cases included first fitting the variable temperature data shown in figure 4. This fit was used to fix the values of p, q, n and ν at 1.341, 1.555, 2.274 and 1.758 respectively. Then the variable strain data shown in figure 6 were used to fix the remaining free parameters in the scaling law and are given in table 1. Two types of fits were made: a global fit that includes all the variable field data shown in figure 6 and a high field fit to the data that only used the data at 7 T and above. For comparison equivalent free parameters for Nb_3Sn are also shown in table 1.

5. Resistivity measurements of $B^*_{c2}(\theta)$

AC transport resistivity measurements were undertaken using an Quantum Design 9 T Physical Property Measurement System at Durham University. Two samples were prepared from an ITER specification PF coils multifilamentary Nb-Ti strand. The first was as-supplied. The second was etched in a bath of dilute nitric acid for a period of 72 hours, leaving only the Nb-Ti filaments. The as-supplied and etched samples were each mounted on an AC transport rotator puck which facilitates resistivity measurements as a function of field up to 9 T, temperature and angle between the axis of the wire and the field. A pair of voltage taps were attached 1 cm apart

Table 2. The values of the Ginzburg-Landau fitting parameter γ from equation 11 for the etched and as-supplied ITER specification Nb-Ti strand at various temperatures.

	$\gamma(6.5\,\mathrm{K})$	$\gamma(7\,\mathrm{K})$	$\gamma(8\,\mathrm{K})$	$\gamma(9\,\mathrm{K})$
Etched	—	0.912	0.878	0.741
As-supplied	0.831	0.783	0.708	—

on the samples. Silver paint was used to connect to the etched sample. Solder was used for the as-supplied wire. Field sweeps were undertaken at temperatures of 6.5 K, 7 K and 8 K for the as-supplied sample and at 7 K, 8 K and 9 K for the etched sample to measure B^*_{c2} at successive angles. The field was ramped at a rate of $2\,\mathrm{mT\,s^{-1}}$, and a transport current of 20 mA was used for both samples. Additional field sweeps were completed at $B \perp I$ and $B \parallel I$ for both samples at 7.5 K and 8.5 K and at 6.5 K for the etched sample. Angular measurements were made from 0° ($B \perp J$) to 95° (5° beyond $B \parallel J$). B^*_{c2} was defined as the field at which the sample resistivity reached 90 % of its normal state resistivity. The results obtained for the upper critical field as a function of the angle between the applied field and the axis of the wire for the etched and non-etched samples are shown in figure 8. A fit to these data using Ginzburg-Landau theory for an anisotropic superconductor [23] was made using

$$B^*_{c2}(\theta) = \frac{B^*_{c2}(0)}{\sqrt{\cos^2(\theta) + \gamma^{-2}\sin^2(\theta)}} \tag{11}$$

where $\gamma = \xi_\parallel/\xi_\perp \propto \left(\rho_\perp/\rho_\parallel\right)^{0.5}$, $\xi_\parallel$ and $\xi_\perp$ are the effective coherence lengths parallel and perpendicular to the sample axis and $\rho_\perp$ and $\rho_\parallel$ are the sample bulk resistivities perpendicular and parallel to the sample axis. The values of the parameter γ for each of the fits are given in table 2. The upper critical fields at $B \perp J$ and $B \parallel J$ for both samples as a function of temperature are plotted in figure 9. Several other data points from previous measurements [24, 25] on Nb 47±1%wtTi strands are also included and show good agreement with the results from this study. Values of $B^*_{c2}(4.2\,\mathrm{K})$ were obtained from the fits to the data and are presented in table 3.

6. Heat capacity measurements of $B^*_{c2}(\theta)$

In order to distinguish bulk properties from surface properties we measured B^*_{c2} of the as-supplied single-filament wire using heat capacity measurements, C_p. We used our Quantum Design PPMS system to make the measurements. Short lengths of the wire were cut and weighed, and then positioned using G.E. varnish on the sample holder at an angle with respect to the direction of the magnetic field. Figure 10 shows heat capacity data for three orientations of the field with respect to the wire axis. Figure 11 shows a summary of the data taken at 8 T which makes clear that the bulk B^*_{c2} is unambiguously higher when the field is parallel to the axis of the single filament as-supplied wire.

7. Optimising the microstructure and composition of Nb-Ti wires

To date, the development of Nb-Ti has primarily focused on increasing its critical current density in fields of $\sim$ 5 T for MRI. This has been achieved by optimising the titanium content to produce almost pure Ti α-Ti precipitates for flux pinning [26] and the optimum Ti content in the superconducting matrix to produce a high B^*_{c2} [27]. Given a precipitate content of almost pure Ti precipitates of 15-20 %, the % weight Ti content in the matrix is $\approx$ 38 % and one can

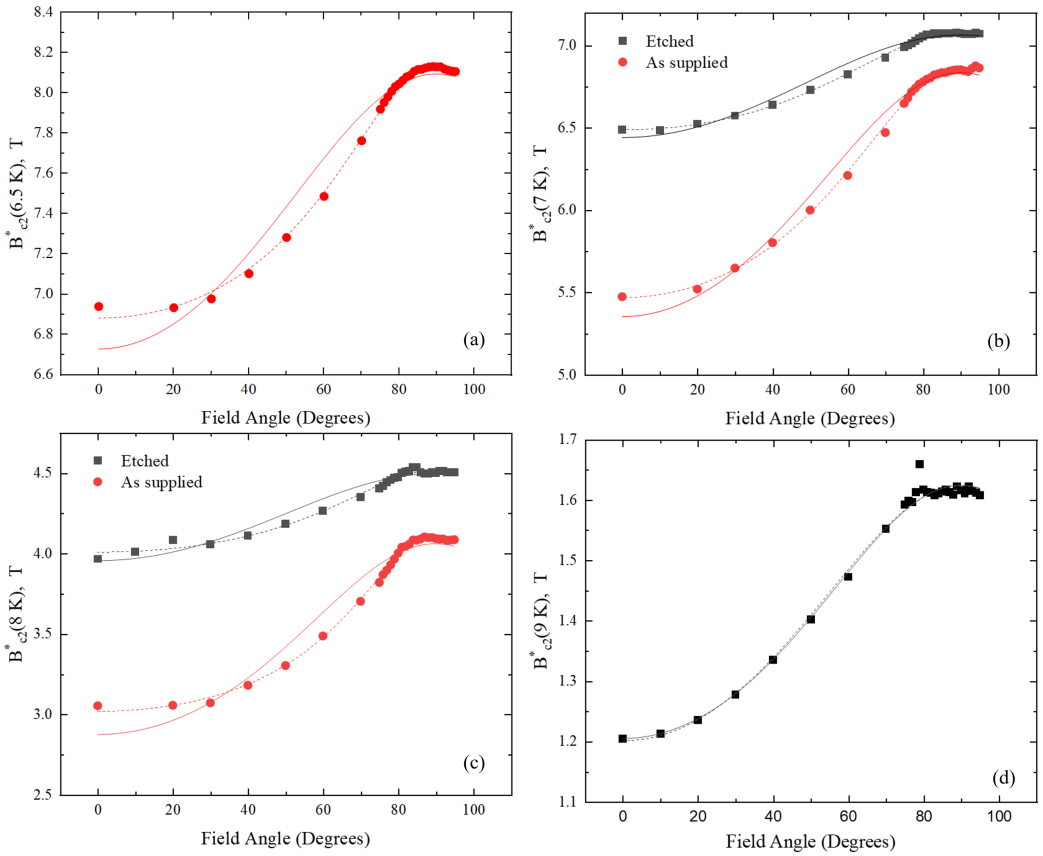

Figure 8. Upper critical field at (a) 6.5 K, (b) 7 K, (c) 8 K and (d) 9 K for an ITER specification Multifilamentary Nb-Ti strand as a function of the angle between the applied field and current through the strand. Circles are for the as-supplied strand, squares are for the etched filaments. The solid line fits are of the form described by equation 11, the dashed fits are guides to the eye.

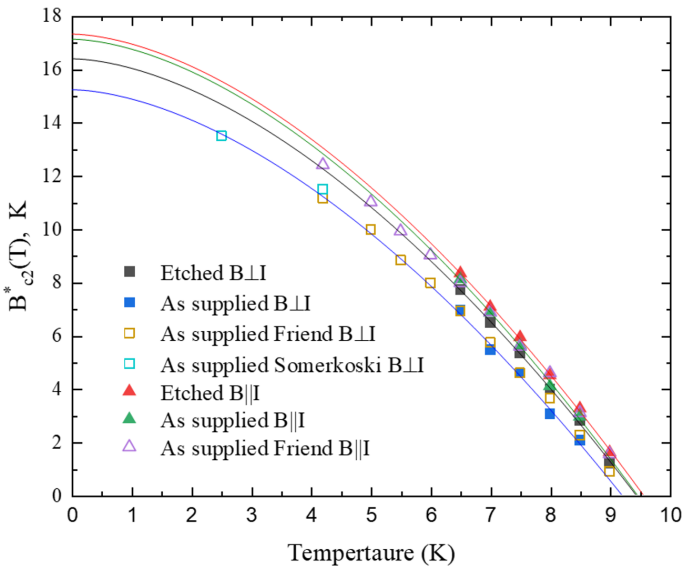

Figure 9. Upper critical field for a single filament as-supplied and etched Nb-Ti wire as a function of temperature for the applied field parallel to (triangles) and perpendicular to (squares) the axis of the wire. The temperature dependence is taken to be of the form in equation 5. Open symbols data are for multifilamentary wires from the literature for Somerkoski [25] and Friend [24].

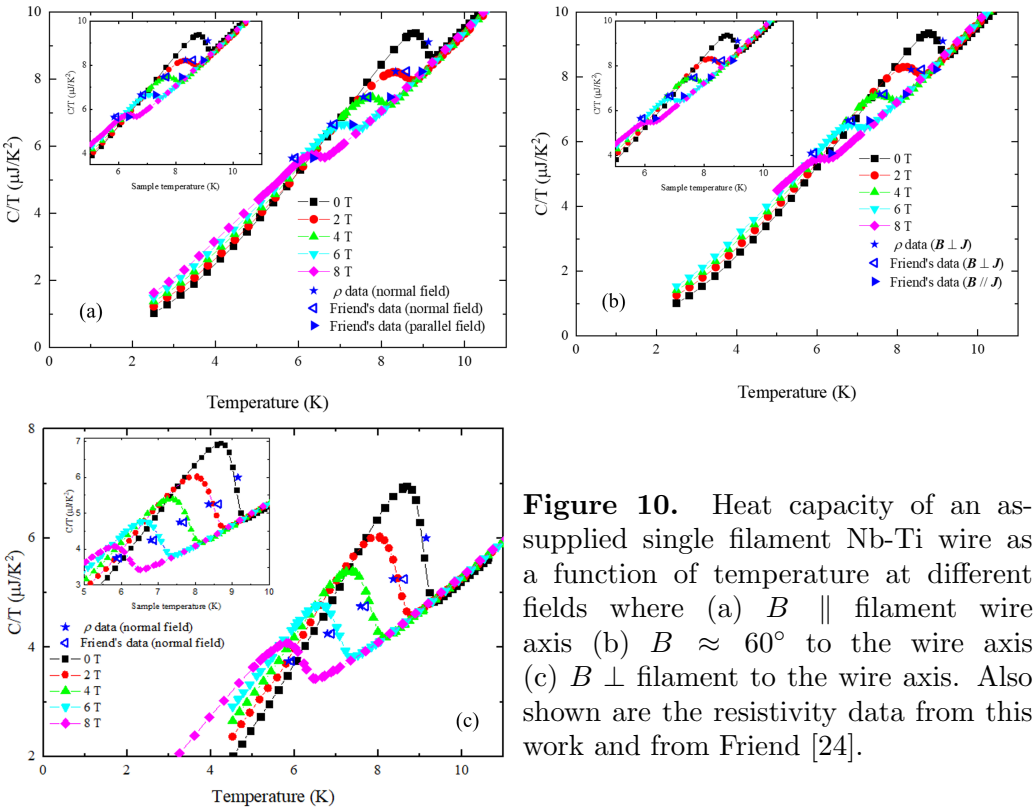

Figure 10. Heat capacity of an as-supplied single filament Nb-Ti wire as a function of temperature at different fields where (a) $B \parallel$ filament wire axis (b) $B \approx 60°$ to the wire axis (c) $B \perp$ filament to the wire axis. Also shown are the resistivity data from this work and from Friend [24].

Table 3. The upper critical field of the etched and the as-supplied multifilamentary, ITER specification Nb-Ti strand at various temperatures. The extrapolation to 4.2 K was performed using a fit of the form given in equation 5 (with $\nu = 1.76$) to the data measured at 6.5 K, 7 K, 8 K and 9 K.

	B^*_{c2}(4.2 K) (T)	B^*_{c2}(6.5 K) (T)	B^*_{c2}(7 K) (T)	B^*_{c2}(8 K) (T)	B^*_{c2}(9 K) (T)
Etched $B \parallel J$	13.01	8.33	7.07	4.50	—
Etched $B \perp J$	12.22	7.71	6.49	3.97	—
As-supplied $B \parallel J$	12.79	8.11	6.85	4.09	1.61
As-supplied $B \perp J$	11.18	6.94	5.47	3.05	1.20

expect that other Ti- content compositions may be more effective for producing high J_c at 10 T where the fluxon-fluxon spacing is smaller. Other potential avenues for the improvement of B^*_{c2} and J_c in Nb-Ti based strands include introducing artificial pinning centres into the superconducting matrix [28] and the use of quaternary alloys. In ternary alloys there is very little improvement in B^*_{c2} at 4.2 K [29, 30, 31], however the quaternary Nb 38.5%wtTi 6.1%wtZr 24.3%wtTa has a significantly higher B^*_{c2}(4.2 K) than binary material, namely 13.1 T [32, 33]. If this value of B^*_{c2}(4.2 K) is used in the scaling laws, keeping the other parameters fixed at those given in table 1, we obtain $J_{c,TS}(4.2\,\mathrm{K}, 10\,\mathrm{T}) \approx 50 - 100\,\mathrm{A\,mm^{-2}}$.

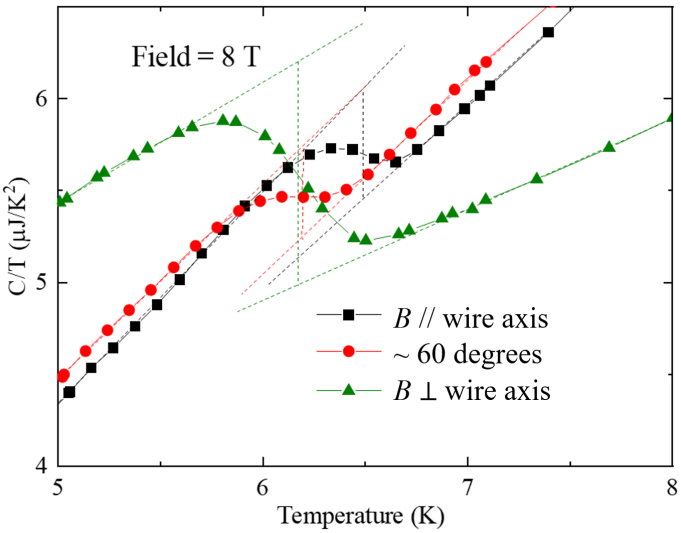

Figure 11. Heat capacity of an as-supplied single filament Nb-Ti wire as a function of temperature and angle between an applied field of 8 T and the wire axis. Dotted lines are guides to the eye.

8. Discussion and conclusions

Extensive $J_c(B, T, \varepsilon)$ data have been provided and fitted with a combination of a standard scaling law and both a simple polynomial as well as the Bordini exponential strain model for $B^*_{c2}(\varepsilon)$. The polynomial is more accurate for interpolating between J_c measurements, which makes it useful for magnet designers where one can expect that that the magnet operates in conditions that have been explicitly measured in characterising the strain. However it has a relatively high number of free parameters and can predict non-physical behaviour when extrapolated out to the highest strains beyond those measured. The exponential model of Bordini is preferred for computational work (equations 2 - 8 and 10) because it is reasonably accurate at high fields and most importantly ensures that at high strains J_c falls to zero. Angular resistive, J_c and C_p measurements are also presented that remind us about the complexity of distinguishing bulk properties from surface properties. The J_c and C_p measurements provide bulk properties and confirm that the angular increases in B^*_{c2} observed in the as-supplied wire when the field is applied along the wire is an increase in a bulk property. We attribute the increase to the layered structure produced by Ti- ribbons with high resistivity in a Nb-Ti matrix. The J_c data in the Lorentz force free condition ($B \parallel J$) show the strength of the pinning is markedly greater than for $B \perp J$ and $B^*_{c2}(4.2\,\mathrm{T})$ is $\approx 1\,\mathrm{T}$ greater as a result. The resistivity measurements on the as-supplied and etched samples show that $B^*_{c2}(\theta)$ strongly depends on the surface conditions of the superconducting filaments. In the as-supplied wire where the metallic copper matrix is in intimate contact with the Nb-Ti material, the surface of the superconductor has a lower B^*_{c2} than the bulk so the angular resistivity measurements are those of the bulk material. After etching however, there is an increase in B^*_{c2} at the superconducting-insulating interface and the angular measurement is now that of the surface. Etched Nb-Ti strands show a $B^*_{c2} \approx 0.2 - 1\,\mathrm{T}$ greater than as-supplied Nb-Ti wire. We also make the case for more work directed at re-optimising Nb-Ti for use in high field tokamak applications both by changing the Ti- content of the Nb-Ti, and perhaps using quaternary alloys with artificial pinning centres. It seems to the authors that further improvements in Nb-Ti for fusion applications are available and inevitable given that higher B^*_{c2} is clearly possible. Whether Nb-Ti can be improved sufficiently that a commercial tokamak can be produced that has the increased reliability that operating a ductile superconductors alone brings, is at present an open question.

Acknowledgments
This work is funded by EPSRC grant EP/L01663X/1 that supports the EPSRC Centre for Doctoral Training in the Science and Technology of Fusion Energy. This work has been carried out within the framework of the EUROfusion Consortium. The data are available at: http://dx.doi.org/ 10.15128/r2qv33rw65q and associated materials are on the Durham Research Online website: http://dro.dur.ac.uk/. We wish to thank Dr M J Raine for his technical expertise and assistance producing Figure 1 and Mr C Gurnham for his proof-reading assistance.

References
[1] Uglietti D, Sedlak K, Wesche R, Bruzzone P, Muzzi L and dellaCorte A 2018 *Supercond. Sci. Technol.* **31** 055004
[2] Wesche R, Sarasola X, Sedlak K, Bykovsky N, Stepanov B, Uglietti D and Bruzzone P 2018 *IEEE Trans. Appl. Supercond.* **28** 4203605
[3] Buxton P F, Connor J W, Costley A E, Gryaznevich M P and McNamara S 2019 *Plasma Phys. Control. Fusion* **61** 035006
[4] Sorbom B N and *et al* 2015 *Fusion Eng. Des.* **100** 378–405
[5] Sykes A and *et al* 2018 *Nucl. Fusion* **58** 016039
[6] Chislett-McDonald S B L, Surrey E and Hampshire D P 2019 *IEEE Trans. Appl. Supercond.* **29** 4200405–8
[7] Bordini B, Alknes P, Bottura L, Rossi L and Valentinis D 2013 *Supercond. Sci. Technol.* **26** 075014
[8] Kovari M, Fox F, Harrington C, Kembleton R, Knight P, Lux H and Morris J 2016 *Fusion Eng. Des.* **104** 9–20
[9] Kovari M, Kemp R, Lux H, Knight P, Morris J and Ward D J 2014 *Fusion Eng. Des.* **89** 3054–69
[10] Boutboul T, Readman P, Viladiu E, Losasso M, Caballero J, Abou-Yehia J and Batista R 2014 *IEEE Trans. Appl. Supercond.* **24** 6001004
[11] 2014 Superconducting magnet technology for fusion and large scale applications `https://www.pppl.gov/sites/pppl/files/Superconducting_Magnet_Technology_for_Fusion_and_Large_Scale_Applications.pdf` [Online; accessed 09-Mar-2020]
[12] 2019 Icas r&d, hts cables for high field magnets `https://www.icasweb.com/r_d.html` [Online; accessed 10-Mar-2020]
[13] Ekin J W 1987 *IEEE Trans. Magn.* **23** 1634–7
[14] Taylor D M J and Hampshire D P 2005 *Supercond. Sci. Technol.* **18** 356–68
[15] Cheggour N and Hampshire D P 2000 *Rev. Sci. Instrum.* **71** 4521
[16] Keys S A and Hampshire D P 2003 *Supercond. Sci. Technol.* **16** 1097–108
[17] Lu X F, Taylor D M J and Hampshire D P 2008 *Supercond. Sci. Technol.* **21** 105016
[18] Taylor D M J and Hampshire D P 2005 *Supercond. Sci. Technol.* **18** S241–52
[19] Dew-Hughes D 1974 *Philos. Mag.* **30** 293–305
[20] Wilson M N 1986 *Superconducting Magnets* (Oxford, UK: Oxford University Press)
[21] Tilley D R and Tilley J 1990 *Superfluids: An Introduction* (Bristol: IOP publishing Ltd.) p 18 3rd ed
[22] Gray W H and Sun C T 1976 Theoretical and experimental determination of mechanical properties of superconducting composite wire Report Oak Ridge National Laboratory
[23] Blatter G, Geshkenbein V B and Larkin A I 1992 *Phys. Rev. Lett.* **68** 875–8
[24] Friend C M and Hampshire D P 1993 *Appl. Supercond.* 23–6
[25] Somerkoski J, Hampshire D, Jones H, Toivanen R and Lindroos V 1987 *IEEE Trans. Magn.* **23** 1629–33
[26] Cooley L D, Lee P and Larbalestier D C 2002 *Processing of Low-T_c Conductors: the Alloy Nb-Ti* vol 1 (Bristol: IOP Publishing) pp 603–38
[27] Muller H J 1989 *The Upper Critical Field of Niobium-Titanium* Thesis University of Wisonsin-Madison
[28] Cooley D L and Motowildo L R 1999 *Supercond. Sci. Technol.* **12** R135–51
[29] Hawksworth D G and Larbalestier D C 1980 *Enhanced Values of H_{c2} in Nb-Ti Ternary and Quaternary Alloys* (Boston, MA: Springer US) pp 479–86
[30] Lee P J, Larbalestier D C, McKinnell J C and McInturff A D 1993 *IEEE Trans. Appl. Supercond.* **3** 1354–7
[31] Watanabe K, Noto K and Muto Y 1991 *TEION KOGAKU (Journal of Cryogenics and Superconductivity Society of Japan)* **26** 120–5
[32] Collings E W 1986 *Applied Superconductivity, Metallurgy, and Physics of Titanium Alloys. Volume 1: Fundamentals* (New York: Plenum Press)
[33] Horiuchi T, Monju Y and Nagai N 1973 *J. Japan Inst. Metals* **37** 882–7